Two-Dimensional Frequency Domain Second-Order Keystone Transform for Weak Target Integration Detection Based on Bistatic Radar Configuration

Zehua LEI [1], Xuan RAO [1], Pan JIN [1,2], Hong YI [1], Jianfen HU [1*]*

[1] Nanchang Hangkong University, 696 South Fenghe Avenue, 330063 Nanchang, China
[2] Sungrow Company, 1699 Xiyou Avenue, High-tech Zone, 230000 Hefei, China

leizehua0@163.com, raoxuancom@163.com, jinpan1992@163.com, hongyi_rsp2021@163.com, ffeenn777@163.com

Submitted September 10 2022 / Accepted December 23, 2022 / Online first March 6, 2023

Abstract. *In this paper, a novel coherent integration algorithm, i.e., two-dimensional frequency domain second-order keystone transform (FDSOKT), is proposed to detect a weak maneuvering target based on bistatic radar configuration. To eliminate range migration and Doppler frequency migration, the radar echoes are transformed into two-dimensional frequency domain firstly, and then a series of rescaling transforms, matched filter functions and compensation functions are performed respectively. With the elimination of the couplings between range frequency and azimuth frequency caused by radial velocity and acceleration, the energy of the echoes is focused in two-dimensional time domain, which improves the detection performance of weak target. In addition, to deal with Doppler ambiguity, different Doppler ambiguity cases are discussed and could be solved well. At last, some simulation experiments are provided and the effectiveness of FDSOKT is proved by the results.*

Keywords

Bistatic radar, range migration, Doppler frequency migration, second-order keystone transform, Doppler ambiguity, two-dimensional frequency domain

1. Introduction

With the rapid development of technology, radar cross-section (RCS) of stealth aircrafts is reduced greatly, which threatens radar systems and affects radar detection performance. To improve the capability of detecting these targets, long time coherent integration is an effective method [1–3]. However, range migration (RM) and Doppler frequency migration (DFM) are inevitable during long time observing weak maneuvering target [4]. Hence, compensating RM and DFM is very important.

To solve RM, some effective algorithms have been proposed, such as Keystone transform (KT) [5–9], Radon Fourier transform (RFT) [10], [11] and axis rotation moving target detection (AR-MTD) [12] and so on. Without a prior knowledge of moving targets, KT can correct range walk (RW), which is induced by target's radial velocity. RFT overcomes RW by Radon transform i.e., jointly searching along range and velocity dimensions and realizes coherent integration via Fourier transform. AR-MTD eliminates RW by rotating two-dimensional echoes data plane and realizes coherent integration via MTD. In addition, second-order Keystone transform (SOKT) [13], [14] is proposed to compensate the range curvature (RC), which is induced by target's radial acceleration. To compensate RM and DFM simultaneously, Generalized Radon-Fourier transform (GRFT) [15], [16], Radon-Fractional Fourier transform (RFRFT) [17], [18] and Radon-Lv's distribution (RLVD) [19], [20] etc. are proposed respectively. Due to the high speed motion of targets or the relative low pulse repetition frequency (PRF) of the radar, Doppler ambiguity, which seriously deteriorates the detection performance, happens frequently and should be taken into consideration.

Compared with monostatic radar, bistatic radar has the advantages of flexible configuration, longer detection range, better anti-stealth and anti-interference ability. Thereby, based on bistatic radar configuration, a novel weak target integration detection algorithm in frequency domain is proposed in this paper, i.e., frequency domain second-order keystone transform (FDSOKT). Similar to SOKT, FDSOKT can eliminate RM via applying different rescaling transforms in the two-dimensional (2-D) frequency domain and can compensate DFM via constructing phase matched function. The remainder of this paper is organized as follows. The target's motion model and the signal model are given in Sec. 2. In Sec. 3, the principle of FDSOKT algorithm is introduced. Finally, some simulation results and conclusions are provided in Sec. 4 and Sec. 5, respectively.

2. Bistatic Radar Signal Model

Suppose that the radar transmits a linear frequency modulated (LFM) pulse signal $s(t)$, which modulated by

DOI: 10.13164/re.2023.0160

radar carrier frequency f_c, may be written as

$$s(t) = p(t)\exp\left(j\pi k_r t^2\right)\exp\left(j2\pi f_c t\right) \tag{1}$$

where $p(t) = \text{rect}\left(\frac{t}{T_p}\right) = \begin{cases} 1, & |t| \le T_p/2 \\ 0, & |t| \le T_p/2 \end{cases}$, t is time, T_p is pulse duration, k_r indicates the frequency rate of the LFM signal.

A general bistatic radar geometry is shown in Fig. 1. In *XOY* plane, P is a moving target with a constant acceleration a and an initial velocity V, T is a radar transmitter, R is a radar receiver. R_t and R_r are the initial range from the transmitter and receiver to the target respectively. α is the angle between the target moving direction and x axis, β is the bistatic angle, and δ is the angle between the target moving direction and the bistatic angle bisector. The instantaneous range sum $R(t_m)$ between the point target and the radar may be written as

$$\begin{aligned} R(t_m) &= R_t(t_m) + R_r(t_m) \\ &= \sqrt{\begin{array}{l} R_t^2 + (Vt_m + \frac{1}{2}at_m^2)^2 \\ -2R_t\left(Vt_m + \frac{1}{2}at_m^2\right)\cos\left(\delta - \frac{\beta}{2}\right) \end{array}} \\ &+ \sqrt{\begin{array}{l} R_r^2 + (Vt_m + \frac{1}{2}at_m^2)^2 \\ -2R_r\left(Vt_m + \frac{1}{2}at_m^2\right)\cos\left(\delta + \frac{\beta}{2}\right) \end{array}} \end{aligned} \tag{2}$$

where t_m is slow time. $R_t(t_m)$, $R_r(t_m)$ and R_t, R_r are the instantaneous range and initial range from the transmitter and receiver to the target respectively.

Perform Taylor series expansion at $t_m = 0$ and then (2) may be written approximately as

$$R(t_m) \approx R_t + R_r - 2V_r t_m + a_e t_m^2 \tag{3}$$

where the radial velocity V_r and the equivalent acceleration a_e are defined as follows.

$$V_r = V\cos\delta\cos\frac{\beta}{2}, \tag{4}$$

$$\begin{aligned} a_e = &\frac{V^2\sin\left(\delta - \frac{\beta}{2}\right)^2}{2R_t} + \frac{V^2\sin\left(\delta + \frac{\beta}{2}\right)^2}{2R_r} \\ &-a\cos\delta\cos\left(\frac{\beta}{2}\right). \end{aligned} \tag{5}$$

After coherent demodulation, the two-dimensional received baseband signal may be given as

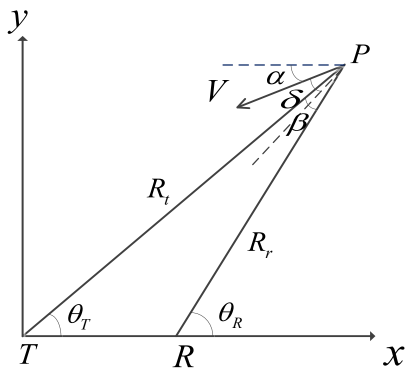

Fig. 1. Bistatic radar geometry.

$$\begin{aligned} s_r(\hat{t}, t_m) = &p\left(\hat{t} - \frac{R(t_m)}{c}\right)\exp\left(j\pi k_r\left(\hat{t} - \frac{R(t_m)}{c}\right)^2\right) \\ &\times\exp\left(-j\frac{2\pi f_c R(t_m)}{c}\right) \end{aligned} \tag{6}$$

where $\hat{t}$ is fast time and $t = \hat{t} + t_m$, c is the speed of electromagnetic wave. After pulse compression (PC) and substituting (3) into (6), the echoes may be represented as

$$\begin{aligned} s_r'(\hat{t}, t_m) = &A\,\text{sinc}\left(B\left(\hat{t} - \frac{1}{c}\left(R_r + R_t - 2V_r t_m + a_e t_m^2\right)\right)\right) \\ &\times\exp\left(-j\frac{2\pi f_c}{c}\left(R_r + R_t - 2V_r t_m + a_e t_m^2\right)\right) \end{aligned} \tag{7}$$

where A is the constant complex amplitude of the echoes, $B = k_r \times T_p$ is the bandwidth of the transmitted signal.

According to (7), it can be observed that RW and RC are all happening. And the instantaneous Doppler frequency of the target can be written as

$$f_d(t_m) = -\frac{1}{\lambda}\frac{dR(t_m)}{dt_m} = \frac{2V_r - 2a_e t_m}{\lambda}. \tag{8}$$

From (8), it is shown that the Doppler frequency is time-varying, which will cause DFM inevitably.

3. Proposed Algorithm

3.1 Case of No Doppler Ambiguity

Perform Fourier transform along fast time dimension on (7) and then the echoes in range frequency-slow time domain can be written as

$$S_{rm}(f_r, t_m) = |P(f_r)|^2\exp\left(-j\frac{2\pi R(t_m)}{c}(f_r + f_c)\right) \tag{9}$$

where f_r is the range frequency.

Then, based on principle of stationary phase [21], (9) may be transformed into 2-D frequency domain via FT (i.e., range frequency-azimuth frequency domain)

$$S_{\mathrm{ra}}(f_{\mathrm{r}},f_{\mathrm{a}})=\left|P(f_{\mathrm{r}})\right|^2\exp\left(\frac{\mathrm{j}\pi c f_{\mathrm{a}}^2}{2a_{\mathrm{e}}(f_{\mathrm{r}}+f_{\mathrm{c}})}\right)\times\exp\left(-\frac{\mathrm{j}4\pi(f_{\mathrm{r}}+f_{\mathrm{c}})}{c}\left(R_0-\frac{V_{\mathrm{r}}^2}{2a_{\mathrm{e}}}\right)\right)\times\exp\left(-\frac{\mathrm{j}2\pi f_{\mathrm{a}}V_{\mathrm{r}}}{a_{\mathrm{e}}}\right) \quad (10)$$

where f_{a} is the azimuth frequency, initial range sum $R_0 = R_{\mathrm{t}} + R_{\mathrm{r}}$.

From (10), it is shown that there is a coupling between f_{r} and f_{a} in the first exponential term, which brings RC. Similar to time domain SOKT [22], FDSOKT is proposed to correct RC in 2-D frequency domain. Firstly, f_{a} is rescaled to f_{a}' by the following transform (i.e., rescaling transform I):

$$f_{\mathrm{a}}=\sqrt{\frac{f_{\mathrm{r}}+f_{\mathrm{c}}}{f_{\mathrm{c}}}}f_{\mathrm{a}}'. \quad (11)$$

To ensure the rescaling accuracy in frequency domain [23], the number of zeros, which equals the number of pulses, should be added in the $S_{\mathrm{ra}}(f_{\mathrm{r}}, f_{\mathrm{a}})$ along the azimuth frequency domain before FDSOKT is performed. Substituting (11) into (10), we can obtain

$$S_{\mathrm{ra}}'(f_{\mathrm{r}},f_{\mathrm{a}}')=\left|P(f_{\mathrm{r}})\right|^2\times\exp\left(-\frac{\mathrm{j}4\pi(f_{\mathrm{r}}+f_{\mathrm{c}})}{c}\left(R_0-\frac{V_{\mathrm{r}}^2}{2a_{\mathrm{e}}}\right)\right)\times\exp\left(\frac{\mathrm{j}\pi c(f_{\mathrm{a}}')^2}{2a_{\mathrm{e}}f_{\mathrm{c}}}\right)\times\exp\left(-\frac{\mathrm{j}2\pi f_{\mathrm{a}}'\sqrt{\frac{f_{\mathrm{r}}+f_{\mathrm{c}}}{f_{\mathrm{c}}}}V_{\mathrm{r}}}{a_{\mathrm{e}}}\right). \quad (12)$$

It is shown from (12) that the coupling between f_{r} and f_{a} in the first exponential term is eliminated.

Secondly, a frequency domain-matched filter function is constructed as

$$H_1(f_{\mathrm{a}}')=\exp\left(\frac{\mathrm{j}\pi c(f_{\mathrm{a}}')^2}{2a_{\mathrm{e}}f_{\mathrm{c}}}\right). \quad (13)$$

Then, we can have

$$S_{\mathrm{ra}}''(f_{\mathrm{r}},f_{\mathrm{a}}')=S_{\mathrm{ra}}'(f_{\mathrm{r}},f_{\mathrm{a}}')\times H_1^*(f_{\mathrm{a}}')=\left|P(f_r)\right|^2\times\exp\left(-\frac{\mathrm{j}4\pi(f_{\mathrm{r}}+f_{\mathrm{c}})}{c}\left(R_0-\frac{V_{\mathrm{r}}^2}{2a_{\mathrm{e}}}\right)\right)\times\exp\left(-\frac{\mathrm{j}2\pi f_{\mathrm{a}}'\sqrt{\frac{f_{\mathrm{r}}+f_{\mathrm{c}}}{f_{\mathrm{c}}}}V_{\mathrm{r}}}{a_{\mathrm{e}}}\right). \quad (14)$$

According to (14), a new coupling between f_{r} and f_{a}' is introduced in the second exponential term, which shows that RW still exists.

Lastly, rescaling transform II, i.e., $f_{\mathrm{a}}'=\sqrt{\frac{f_{\mathrm{c}}}{f_{\mathrm{r}}+f_{\mathrm{c}}}}f_{\mathrm{a}}''$, is substituted into (14). Then

$$S_{\mathrm{ra}}'''(f_{\mathrm{r}},f_{\mathrm{a}}'')=\left|P(f_{\mathrm{r}})\right|^2\times\exp\left(-\frac{\mathrm{j}4\pi(f_{\mathrm{r}}+f_{\mathrm{c}})}{c}\left(R_0-\frac{V_{\mathrm{r}}^2}{2a_{\mathrm{e}}}\right)\right)\times\exp\left(-\frac{\mathrm{j}2\pi f_{\mathrm{a}}''V_{\mathrm{r}}}{a_{\mathrm{e}}}\right). \quad (15)$$

Compared with (10) and (14), (15) shows that the coupling between f_{r} and f_{a}'' is eliminated and the target could be detected in 2-D time domain after 2-D IFFT.

3.2 Case of Happening Doppler Ambiguity

For high-speed moving targets, Doppler ambiguity may happen [24]. As shown in Fig. 2, Doppler spectrum distributions mainly include two cases: I) the signal spectrum locates entirely in one PRF band; II) the signal spectrum is distributed in two neighboring PRF bands.

I) For Case I, the 2-D spectrum can be retrieved by shifting the spectrum with M PRFs along the azimuth frequency. Substituting $f_{\mathrm{a}} + M \cdot PRF$ for f_{a} in (10), we may have

$$S_{\mathrm{ra}}(f_{\mathrm{r}},f_{\mathrm{a}})=\left|P(f_{\mathrm{r}})\right|^2\exp\left(\frac{\mathrm{j}\pi c(f_{\mathrm{a}}+M\cdot PRF)^2}{2a_{\mathrm{e}}(f_{\mathrm{r}}+f_{\mathrm{c}})}\right)\times\exp\left(-\frac{\mathrm{j}4\pi(f_{\mathrm{r}}+f_{\mathrm{c}})}{c}\left(R_0-\frac{V_{\mathrm{r}}^2}{2a_{\mathrm{e}}}\right)\right)\times\exp\left(-\frac{\mathrm{j}2\pi(f_{\mathrm{a}}+M\cdot PRF)V_{\mathrm{r}}}{a_{\mathrm{e}}}\right). \quad (16)$$

Then, substituting (11) into (16), we can have

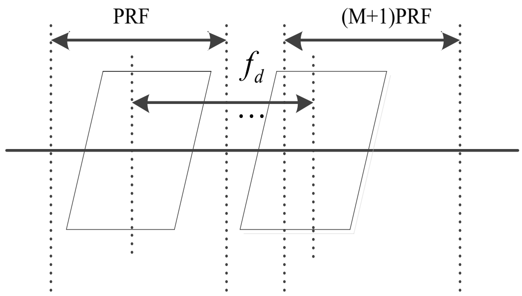

(a)

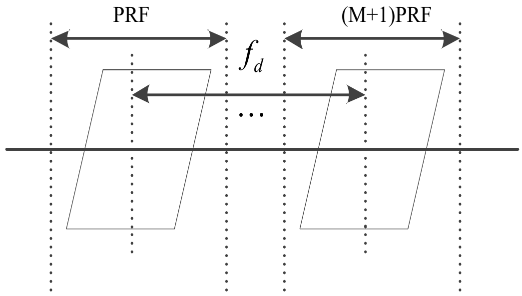

(b)

Fig. 2. Echoes spectrum along azimuth dimension. (a) Case I: spectrum is entirely in a PRF band. (b) Case II: spectrum spans over two adjacent PRF bands.

$$\begin{aligned}S'_{\mathrm{ra}}\left(f_{\mathrm{r}},f'_{\mathrm{a}}\right)=&\left|P\left(f_{\mathrm{r}}\right)\right|^2\exp\left(\frac{\mathrm{j}\pi c f'^{2}_{\mathrm{a}}}{2a_{\mathrm{e}}f_{\mathrm{c}}}\right)\\&\times\exp\left(\frac{\mathrm{j}\pi c\left(M\cdot PRF\right)^2}{2a_{\mathrm{e}}\left(f_{\mathrm{r}}+f_{\mathrm{c}}\right)}\right)\\&\times\exp\left(\frac{\mathrm{j}\pi c f'_{\mathrm{a}}\sqrt{\frac{f_{\mathrm{r}}+f_{\mathrm{c}}}{f_{\mathrm{c}}}}M\cdot PRF}{a_{\mathrm{e}}\left(f_{\mathrm{r}}+f_{\mathrm{c}}\right)}\right)\\&\times\exp\left(-\frac{\mathrm{j}2\pi f'_{\mathrm{a}}\sqrt{\frac{f_{\mathrm{r}}+f_{\mathrm{c}}}{f_{\mathrm{c}}}}V_{\mathrm{r}}}{a_{\mathrm{e}}}\right)\\&\times\exp\left(-\frac{\mathrm{j}4\pi\left(f_{\mathrm{r}}+f_{\mathrm{c}}\right)}{c}\left(R_0-\frac{V_{\mathrm{r}}^2}{2a_{\mathrm{e}}}\right)\right)\\&\times\exp\left(-\frac{\mathrm{j}2\pi M\cdot PRF\cdot V_{\mathrm{r}}}{a_{\mathrm{e}}}\right).\end{aligned}\tag{17}$$

Then, a Doppler ambiguity compensation function is constructed as follows

$$H_2\left(f_{\mathrm{r}},f'_{\mathrm{a}}\right)=\exp\left(\frac{\mathrm{j}\pi c f'_{\mathrm{a}}\sqrt{\frac{f_{\mathrm{r}}+f_{\mathrm{c}}}{f_{\mathrm{c}}}}M\cdot PRF}{a_{\mathrm{e}}\left(f_{\mathrm{r}}+f_{\mathrm{c}}\right)}\right).\tag{18}$$

The ambiguity number M could be well estimated by [25], [26]. Therefore, after match filtering and Doppler ambiguity compensating, we can have

$$\begin{aligned}S''_{\mathrm{ra}}\left(f_{\mathrm{r}},f'_{\mathrm{a}}\right)=&S\left(f_{\mathrm{r}},f'_{\mathrm{a}}\right)\times H_1^*\left(f'_{\mathrm{a}}\right)\times H_2\left(f_{\mathrm{r}},f'_{\mathrm{a}}\right)\\=&\left|P\left(f_{\mathrm{r}}\right)\right|^2\exp\left(\frac{\mathrm{j}\pi c\left(M\cdot PRF\right)^2}{2a_{\mathrm{e}}\left(f_{\mathrm{r}}+f_{\mathrm{c}}\right)}\right)\\&\times\exp\left(-\frac{\mathrm{j}2\pi M\cdot PRF\cdot V_{\mathrm{r}}}{a_{\mathrm{e}}}\right)\\&\times\exp\left(-\frac{\mathrm{j}4\pi\left(f_{\mathrm{r}}+f_{\mathrm{c}}\right)}{c}\left(R_0-\frac{V_{\mathrm{r}}^2}{2a_{\mathrm{e}}}\right)\right)\\&\times\exp\left(-\frac{\mathrm{j}2\pi f'_{\mathrm{a}}\sqrt{\frac{f_{\mathrm{r}}+f_{\mathrm{c}}}{f_{\mathrm{c}}}}V_{\mathrm{r}}}{a_{\mathrm{e}}}\right).\end{aligned}\tag{19}$$

Because of Doppler ambiguity, the last term in (19) may be rewritten as $\exp\left(-\frac{\mathrm{j}\pi c f'_{\mathrm{a}}\sqrt{\frac{f_{\mathrm{r}}+f_{\mathrm{c}}}{f_{\mathrm{c}}}}\left(f_{\mathrm{d\_un}}+M\cdot PRF\right)}{a_{\mathrm{e}}f_{\mathrm{c}}}\right)$, where $f_{\mathrm{d\_un}}$ represents the unambiguity Doppler frequency. Therefore, another Doppler ambiguity term $H_3\left(f_{\mathrm{r}},f'_{\mathrm{a}}\right)=\exp\left(-\frac{\mathrm{j}\pi c f'_{\mathrm{a}}\sqrt{\frac{f_{\mathrm{r}}+f_{\mathrm{c}}}{f_{\mathrm{c}}}}M\cdot PRF}{a_{\mathrm{e}}f_{\mathrm{c}}}\right)$ should be compensated firstly by its conjugation term. Subsequently, $f'_{\mathrm{a}}=\sqrt{\frac{f_{\mathrm{c}}}{f_{\mathrm{r}}+f_{\mathrm{c}}}}f''_{\mathrm{a}}$ is substituted into (19), and we can have

$$\begin{aligned}S'''_{\mathrm{ra}}\left(f_{\mathrm{r}},f''_{\mathrm{a}}\right)=&\left|P\left(f_{\mathrm{r}}\right)\right|^2\exp\left(\frac{\mathrm{j}\pi c\left(M\cdot PRF\right)^2}{2a_{\mathrm{e}}\left(f_{\mathrm{r}}+f_{\mathrm{c}}\right)}\right)\\&\times\exp\left(-\frac{\mathrm{j}2\pi M\cdot PRF\cdot V_{\mathrm{r}}}{a_{\mathrm{e}}}\right)\\&\times\exp\left(-\frac{\mathrm{j}4\pi\left(f_{\mathrm{r}}+f_{\mathrm{c}}\right)}{c}\left(R_0-\frac{V_{\mathrm{r}}^2}{2a_{\mathrm{e}}}\right)\right)\\&\times\exp\left(-\frac{\mathrm{j}\pi f''_{\mathrm{a}}f_{\mathrm{d\_un}}}{a_{\mathrm{e}}}\right).\end{aligned}\tag{20}$$

It can be shown from (20) that RM and DFM have been removed together.

II) Compared with the Case I, the signal spectrum in Case II is composed of two parts: the first part is located in the Mth PRF band and the second part is in the $(M+1)$th PRF, which is shown in Fig. 2(b). If Doppler band is less than PRF/2, the signal spectrum will locate in a single PRF band after shifting the spectrum with PRF/2.

Thus, a compensation function is constructed as

$$H_4\left(f_r,t_m\right)=\exp\left(\frac{j\pi\cdot PRF\left(f_r+f_c\right)t_m}{2f_c}\right). \tag{21}$$

Then, we can have

$$\begin{aligned} S_{rm}^{'}\left(f_r,t_m\right) &= S_{rm}\left(f_r,t_m\right)\times H_4\left(f_r,t_m\right) \\ &= \left|P\left(f_r\right)\right|^2 \\ &\times\exp\left(-j\frac{2\pi\left(R_r+R_t\right)}{c}\left(f_r+f_c\right)\right) \\ &\times\exp\left(\frac{j4\pi\left(f_r+f_c\right)}{c}\left(V_r+\frac{\lambda\cdot PRF}{8}\right)t_m\right) \\ &\times\exp\left(-\frac{j2\pi\left(f_r+f_c\right)}{c}a_e t_m^2\right). \end{aligned} \tag{22}$$

Perform FFT on (22) along slow time dimension and adopt the similar processing steps in Case I to deal with the RM and DFM. Subsequently, let $V'_r = V_r + \lambda\cdot PRF/8$, the spectrum in 2-D frequency domain can be written as

$$\begin{aligned} S_{ra}^{'''}\left(f_r,f_a^{''}\right) &= \left|P\left(f_r\right)\right|^2\exp\left(\frac{j\pi c\left(M\cdot PRF\right)^2}{2a_e\left(f_r+f_c\right)}\right) \\ &\times\exp\left(-\frac{j2\pi M\cdot PRF\cdot V_r^{'}}{a_e}\right) \\ &\times\exp\left(-\frac{j4\pi\left(f_r+f_c\right)}{c}\left(R_0-\frac{V_r^{'2}}{2a_e}\right)\right) \\ &\times\exp\left(-\frac{j\pi f_a^{''}f_{d\_un}}{a_e}\right). \end{aligned} \tag{23}$$

Finally, the coupling between f_r and f_a'' is eliminated and the target could be detected in 2-D time domain after 2-D IFFT. Based on the analysis above, the flowchart of FDSOKT is given in Fig. 3.

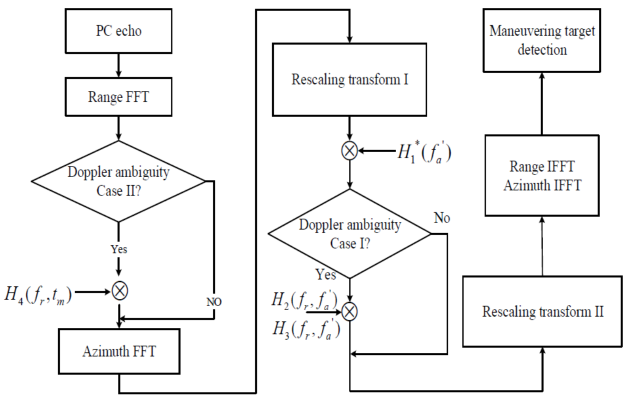

Fig. 3. The flowchart of FDSOKT.

Carrier frequency	5.5 GHz
Pulse repetition frequency	2000 Hz
Pulse width	50 μs
Bandwidth	2 MHz
Coherent integration time	1 s
Sampling frequency	2 MHz
θ_T	π/4 rad
θ_R	25.7π/90 rad
α	π/18 rad

Tab. 1. Simulation parameters.

4. Simulation and Analysis

In this section, some numerical simulations are provided to verify the performance of FDSOKT. According to Fig. 1, suppose that an air moving target with a constant acceleration appears at the coordinate (100 km, 100 km). The transmitter and receiver of radar locate at (0 km, 0 km) and (20 km, 0 km) respectively. The other simulation parameters are given in Tab. 1.

4.1 Weak Target Detection Based on FDSOKT

I) In the first simulation example, suppose that the initial velocity of the target $V = 1020$ m/s, and the acceleration $a = 50$ m/s^2. For the sake of clarity, the FDSOKT algorithm is adopted to detect weak targets without noise. Firstly, the echoes after PC are shown in Fig. 4(a), in which RM is happening. Subsequently, the DFM can be observed in Fig. 4(b) after the echoes are transformed into the Range-Azimuth frequency domain. At the same time, the Doppler frequency of the target is distributed in a PRF band. Then, the FDSOKT algorithm is applied to process the echoes and the RM is eliminated as shown in Fig. 4(c). In Fig. 4(d), a peak of coherent integration is formed in 2-D time domain after DFM has also been compensated.

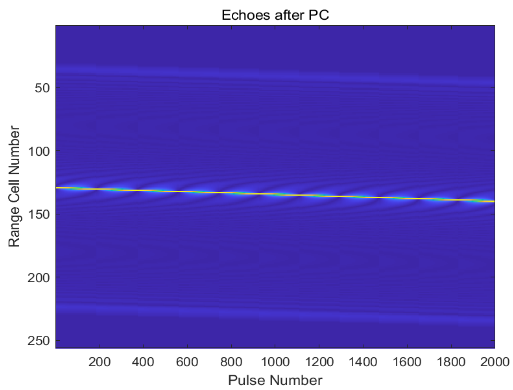

(a)

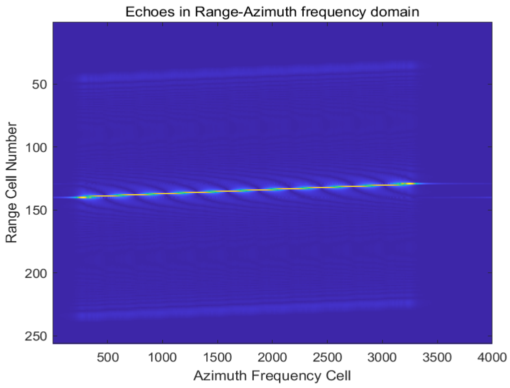

(b)

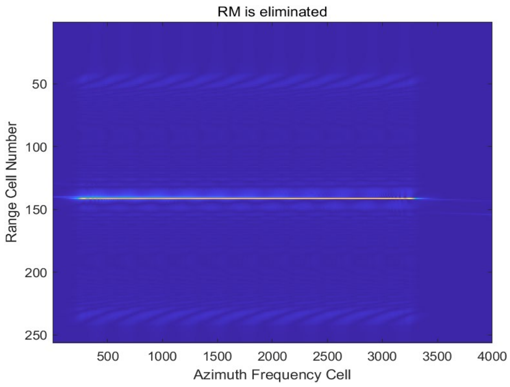

(c)

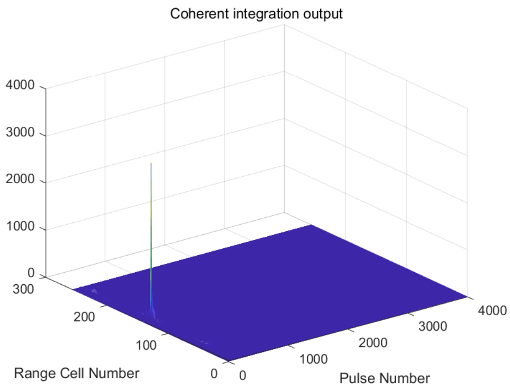

(d)

Fig. 4. Results of FDSOKT without spectrum span. (a) Echoes after PC. (b) Echoes are shown in Range-Azimuth frequency domain. (c) RM is eliminated after performing FDSOKT. (d) Coherent integration output.

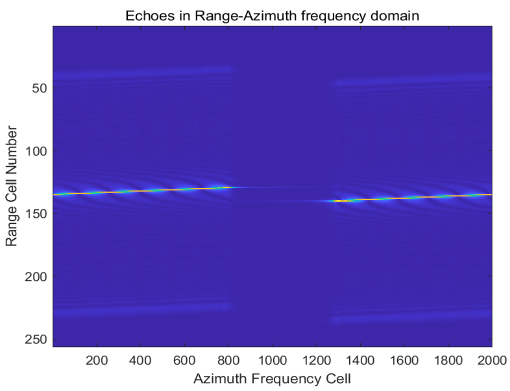

(a)

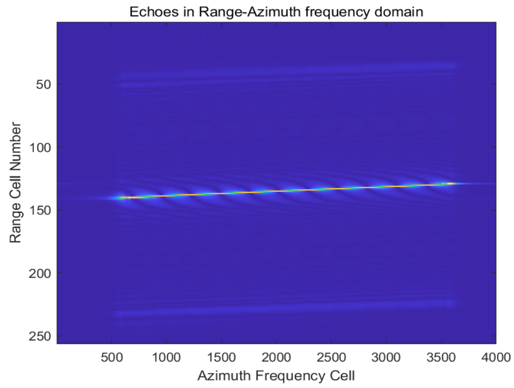

(b)

Fig. 5. Results of FDSOKT with spectrum span. (a) Echoes are shown in Range-Azimuth frequency domain when the spectrum spans over two adjacent PRF bands. (b) Echoes are shown in Range-Azimuth frequency domain after compensating spectrum span.

II) In the second simulation example, suppose that the initial velocity of the target $V = 1049$ m/s, and the acceleration $a = 50$ m/s^2. Compared with the first simulation, Figure 5(a) shows that the echo of the target spans the adjacent PRF band in the Range-Azimuth frequency domain. Subsequently, Figure 5(b) shows that the FDSOKT algorithm applies a compensation function to adjust the Doppler spectrum into a PRF band. Then, the subsequent processing has a same way with the first simulation.

4.2 Comparison of Detection Ability

In the third simulation, the detection performance of SOKT, GRFT, RFRFT, RLVD and FDSOKT are compared.

When the false alarm probability P_{fa} equals 10^{-6} and the number of Monte Carlo trials is 10^2, the detection probabilities of various algorithms under different single pulse input SNRs are shown in Fig. 6(a). When the single pulse input SNR is fixed on −41 dB, the receiver operating characteristic (ROC) curve is given in Fig. 6(b). It is obvious that FDSOKT has a better detection performance than other algorithms.

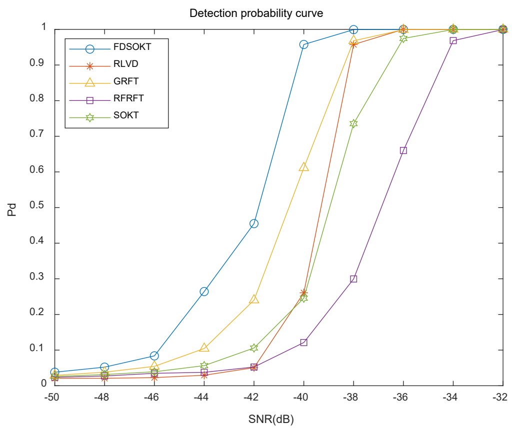

(a)

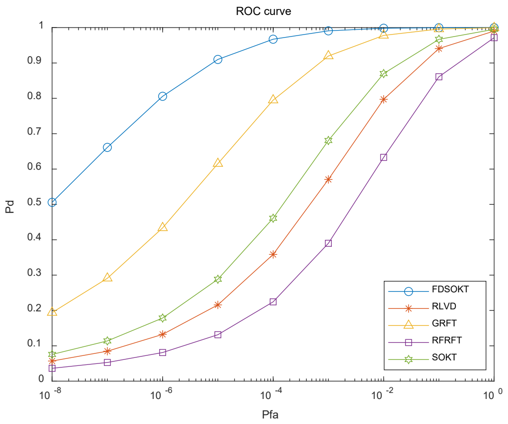

(b)

Fig. 6. Comparison of detection performance. (a) Detection probability curve. (b) ROC curve.

5. Conclusion

Inspired by time domain SOKT, a novel coherent integration algorithm FDSOKT for the detection of weak maneuvering target based on bistatic radar configuration is proposed in this paper. A series of rescaling transforms, matched filter functions and compensation functions are performed respectively in two-dimensional frequency domain to eliminate RM and DFM. Finally, some simulations verify the effectiveness of FDSOKT. Thus, a conclusion may be drawn that for the weak moving target with a constant radial acceleration, FDSOKT has a better detection performance, which benefits from the fact of frequency domain processing having a better ability of anti-noise.

Acknowledgments

The authors would like to thank the reviewers for their valuable comments on the paper. This work is supported by the National Nature Science Foundation of China under Grant 62161029, Jiangxi Provincial Natural Science Foundation under Grants 20202BABL202002, SAST2018078, the Doctoral Scientific Research Foundation of NCHU under Grant EA201804195.

References

[1] LIN, L., SUN, G., CHENG, Z., et al. Long-time coherent integration for maneuvering target detection based on ITRT-MRFT. *IEEE Sensors Journal*, 2020, vol. 20, no. 7, p. 3718–3731. DOI: 10.1109/JSEN.2019.2960323

[2] SUN, Z., LI, X., CUI, G., et al. A fast approach for detection and parameter estimation of maneuvering target with complex motions in coherent radar system. *IEEE Transactions on Vehicular Technology*, 2021, vol. 70, no. 10, p. 10278–10292. DOI: 10.1109/TVT.2021.3104659

[3] CAO, Y.-F., WANG, W.-Q., ZHANG, S. Long-time coherent integration for high-order maneuvering target detection via zero-trap line extraction. *IEEE Transactions on Aerospace and Electronic Systems*, 2021, vol. 57, no. 6, p. 4017–4027. DOI: 10.1109/TAES.2021.3082718

[4] MA, J., HUANG, P., YU, J., et al. An efficient coherent integration method for maneuvering target detection with nonuniform pulse sampling based on filterbank framework. *IEEE Geoscience and Remote Sensing Letters*, 2020, vol. 17, no. 12, p. 2045–2049. DOI: 10.1109/LGRS.2019.2962065

[5] PERRY, R. P., DIPIETRO, R. C., FANTE, R. L. SAR imaging of moving targets. *IEEE Transactions on Aerospace and Electronic Systems*, 1999, vol. 35, no. 1, p. 188–200. DOI: 10.1109/7.745691

[6] ZHU, D., LI, Y., ZHU, Z. A keystone transform without interpolation for SAR ground moving-target imaging. *IEEE Geoscience and Remote Sensing Letters*, 2007, vol. 4, no. 1, p. 18–22. DOI: 10.1109/LGRS.2006.882147

[7] ZHANG, S., ZENG, T. Weak target detection based on keystone transform. *Acta Electronica Sinica*, 2005, vol. 33, no. 9, p. 1675 to 1678. (In Chinese)

[8] DAI, Z., ZHANG, X., FANG, H., et al. High accuracy velocity measurement based on keystone transform using entropy minimization. *Chinese Journal of Electronics*, 2016, vol. 25, no. 4, p. 774–778. DOI: 10.1049/cje.2016.06.009

[9] HUANG, P., LIAO, G., YANG, Z., et al. Long-time coherent integration for weak maneuvering target detection and high-order motion parameter estimation based on keystone transform. *IEEE Transactions on Signal Processing*, 2016, vol. 64, no. 15, p. 4013–4026. DOI: 10.1109/TSP.2016.2558161

[10] YU, J., XU, J., PENG, Y.-N., et al. Radon-Fourier transform for radar target detection (III): Optimality and fast implementations. *IEEE Transactions on Aerospace and Electronic Systems*, 2012, vol. 48, no. 2, p. 991–1004. DOI: 10.1109/TAES.2012.6178044

[11] DING, Z., ZHANG, T., LI, Y., et al. A ship ISAR imaging algorithm based on generalized Radon-Fourier transform with low SNR. *IEEE Transactions on Geoscience and Remote Sensing*, 2019, vol. 57, no. 9, p. 6385–6396. DOI: 10.1109/TGRS.2019.2905863

[12] RAO, X., TAO, H., SU, J., et al. Axis rotation MTD algorithm for weak target detection. *Digital Signal Processing*, 2014, vol. 26, no. 1, p. 81–86. DOI: 10.1016/j.dsp.2013.12.003

[13] ZHOU, F., WU, R., XING, M., et al. Approach for single channel SAR ground moving target imaging and motion parameter estimation. *IET Radar Sonar and Navigation*, 2007, vol. 1, no. 1, p. 59–66. DOI: 10.1049/iet-rsn:20060040

[14] HUANG, P., LIAO, G., YANG, Z., et al. Ground maneuvering target imaging and high-order motion parameter estimation based on second-order keystone and generalized Hough-HAF transform. *IEEE Transactions on Geoscience and Remote Sensing*, 2017, vol. 55, no. 1, p. 320–335. DOI: 10.1109/TGRS.2016.2606436

[15] XU, J., XIA, X. G., PENG, S. B., et al. Radar maneuvering target motion estimation based on generalized Radon-Fourier transform. *IEEE Transactions on Signal Processing*, 2012, vol. 60, no. 12, p. 6190–6201. DOI: 10.1109/TSP.2012.2217137

[16] MA, B., ZHANG, S., JIA, W., et al. Fast implementation of generalized Radon–Fourier transform. *IEEE Transactions on Aerospace and Electronic Systems*, 2021, vol. 57, no. 6, p. 3758–3767. DOI: 10.1109/TAES.2021.3082717

[17] CHEN, X., GUAN, J., LIU, N., et al. Maneuvering target detection via Radon-fractional Fourier transform-based long-time coherent integration. *IEEE Transactions on Signal Processing*, 2014, vol. 62, no. 4, p. 939–953. DOI: 10.1109/TSP.2013.2297682

[18] GAO, C., TAO, R., KANG, X. Weak target detection in the presence of sea clutter using Radon-fractional Fourier transform canceller. *IEEE Journal of Selected Topics in Applied Earth Observations and Remote Sensing*, 2021, vol. 14, p. 5818–5830. DOI: 10.1109/JSTARS.2021.3078723

[19] LI, X., CUI, G., YI, W., et al. Coherent integration for maneuvering target detection based on Radon-Lv's distribution. *IEEE Signal Processing Letters*, 2015, vol. 22, no. 9, p. 1467–1471. DOI: 10.1109/LSP.2015.2390777

[20] LV, X., BI, G., WAN, C., et al. Lv's distribution: principle, implementation, properties, and performance. *IEEE Transactions on Signal Processing*, 2011, vol. 59, no. 8, p. 3576–3591. DOI: 10.1109/TSP.2011.2155651

[21] LI, J., ZHANG, S., CHANG, J. Bistatic forward-looking SAR imaging based on two-dimensional principle of stationary phase. In *The 2012 International Workshop on Microwave and Millimeter Wave Circuits and System Technology*. Chengdu (China), 2012, p. 1–4. DOI: 10.1109/MMWCST.2012.6238129

[22] YANG, J., ZHANG, Y. An airborne SAR moving target imaging and motion parameters estimation algorithm with azimuth-dechirping and the second-order keystone transform applied. *IEEE Journal of Selected Topics in Applied Earth Observations and Remote Sensing*, 2015, vol. 8, no. 8, p. 3967–3976. DOI: 10.1109/JSTARS.2015.2426504

[23] YU, S. P. Frequency domain interpolation problem. *Oil Geophysical Prospecting*, 1981, vol. 4, p. 15–16. ISSN: 1000-7210

[24] HUANG, P., XIA, X., LIAO, G., et al. Long-time coherent integration algorithm for radar maneuvering weak target with acceleration rate. *IEEE Transactions on Geoscience and Remote Sensing*, 2019, vol. 57, no. 6, p. 3528–3542. DOI: 10.1109/TGRS.2018.2885508

[25] ZHU, S., LIAO, G., QU, Y., et al. A new slant-range velocity ambiguity resolving approach of fast moving targets for SAR system. *IEEE Transactions on Geoscience and Remote Sensing*, 2010, vol. 48, no. 1, p. 432–451. DOI: 10.1109/TGRS.2009.2027698

[26] JIN, K., LI, G., LAI, T., et al. A novel long-time coherent integration algorithm for Doppler-ambiguous radar maneuvering target detection. *IEEE Sensors Journal*, 2020, vol. 20, no. 16, p. 9394–9407. DOI: 10.1109/JSEN.2020.2988583

About the Authors …

Zehua LEI was born in Xian, Shaanxi, China, in 1998. He received the B.Eng. degree in Electronics Information Science and Technology from the Xi`an University of Science and Technology in 2018. He is currently pursuing the M.S. degree in Signal Processing from the School of Information Engineering, Nanchang Hangkong University. His current research interests include radar signal processing, and weak target detection.

Xuan RAO was born in Jiangxi Province, P.R. China, in 1977. He received the B.Sc. and M.Sc. degrees from the School of Information Engineering, Nanchang University, Nanchang, China, in 1999 and 2005, respectively; and the Ph.D. degrees from the School of Electronic Engineering, Xidian University, Xi'an, China, in 2015. He is currently an Associate Professor of the School of Information Engineering, Nanchang Hangkong University, China. He is a member of IEEE and his current research interests include radar signal processing, weak target detection and tracking.

Pan JIN was born in Anhui Province, China. He received the B.Eng. degree in Communication Engineering from the Anhui Xinhua University, in 2016. He is currently pursuing the M.S. degree in Signal Processing from the School of Information Engineering, Nanchang Hangkong University. His current research interests include radar signal processing and weak target detection.

Hong YI (*corresponding author) was born in Jiangxi Province, P.R. China, in 1977. She received the Master degree in Computer Science from the School of Measuring and Control Engineering, Nanchang Hangkong University, Nanchang, China, in 2006. She is currently a lecturer of the School of Information Engineering, Nanchang Hangkong University, China. Her current research interests include control theory and control engineering.

Jianfen HU (*corresponding author) was born in Jiangxi Province, P.R. China, in 1978. She received the Master degree from the School of Measuring and Control Engineering, the Northwestern Polytechnical University, Xi'an, China, in 2005. Her current research interests include signal processing, weak target detection and tracking.